Electronic Supplementary Material (ESI) for ChemComm.


# Supplementary Information

# Colorimetric Detection of Acidic Pesticides in Water

Kyle T. Smith, Chloe A. Ramsperger, Kye E. Hunter, Tim Zuehlsdorff, Kyriakos C. Stylianou*

Department of Chemistry, Oregon State University, 153 Gilbert Hall, Corvallis OR 97331

Email: kyriakos.stylianou@oregonstate.edu

## 1. Experimental

### 1.1: Materials

All chemicals were purchased from Sigma Aldrich, Avantor, VWR, MilliporeSigma, and Tokyo Chemical Industry and used without further purification. Powder X-ray diffraction data were collected on a Rigaku MiniFlex XRD using Cu Kα radiation (λ = 1.5418 Å, 50 kW/40mA). Simulated powder X-ray diffraction patterns were generated from the single crystal data using Mercury 3.0. Thermogravimetric analysis (TGA) was performed in argon on a Shimadzu Thermogravimetric Analyzer (TGA) with a heating rate of 10ºC/min. Infrared spectra were collected on a Spectrum Two FTIR Spectrometer (PerkinElmer) from 400 to 4000 $cm^{-1}$. UV/vis absorption spectra were obtained with a Lambda 950S PerkinElmer UV/vis Spectrometer.

### 1.2: Synthesis of MOF-545

MOF-545 was synthesized based on reported procedures,[1] as follows:
Zirconyl chloride octahydrate (75 mg, 0.32 mmol), tetrakis(4-carboxyphenyl)porphyrin (50 mg, 0.063 mmol) was added to the solution, and Benzoic acid (2.7 g, 22 mmol) were weighed out and transferred to a 6-dram vial. Following that, 8 mL of DMF was added to the vial, and the solution was sonicated for ten minutes. The 6-dram vial was at 120 °C for 48 hours. Purple crystals were collected by filtration and washed with DMF.

### 1.3: Characterization Methods

The **powder X-ray diffraction patterns (PXRD)** were recorded on a Rigaku MiniFlex XRD diffractometer using monochromated Cu Kα radiation (λ= 1.5418 Å) at ambient temperature. Our conditions of measurement was from 3 to 30 degrees, with a step of 0.02 degrees and a speed of 0.5°/min. Voltage was 40 kV and the current was 15 mA.

The **thermogravimetric analysis (TGA)** was carried out with a Shimadzu Thermogravimetric Analyzer (TGA) under argon atmosphere, at a heating rate of 10 °C/min up to 600 °C for all measurements.

The **UV-Vis absorbance** spectra were obtained using a PerkinElmer UV-Vis Spectrometer. The diffuse reflectance was collected by depositing the powders within quartz slides and the Kubelka-Munk function was applied to the raw data in order to eliminate scattering.

**Fourier-transform infrared spectroscopy (FT-IR)** was conducted on a PerkinElmer Spectrum Two FTIR Spectrometer.

**Nitrogen adsorption-desorption isotherms** were collected at 77K and 1 bar using the 3FLEX. Before collecting data, the samples were degassed at 130 °C for 12 h. The BET surface areas were estimated from the amount of $N_2$ adsorbed via the BET (Brunauer-Emmett-Teller) equilibrium equation.

## 2. Characterization for MOF-545

### 2.1: Powder X-ray Diffraction (PXRD)

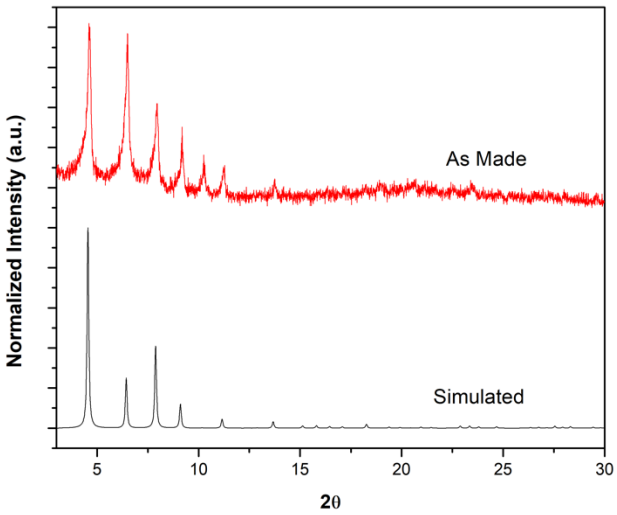


**Fig. S1**: Powder X-ray patterns of the calculated (gray) and the synthesized MOF-545 (Red).

### 2.2: FT-IR

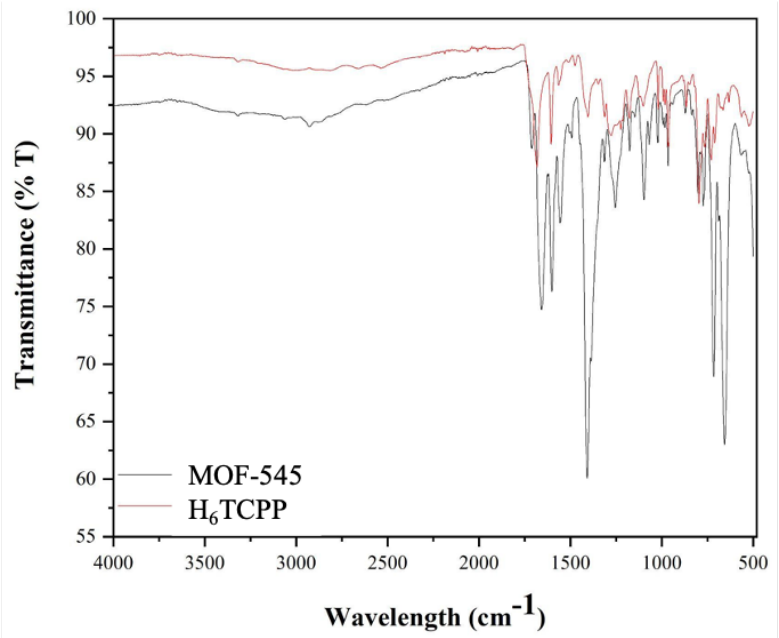


**Fig. S2**: FT-IR of MOF-545 compared to the IR of $H_6$TCPP.

## 2.3: Thermogravimetric Analysis (TGA)

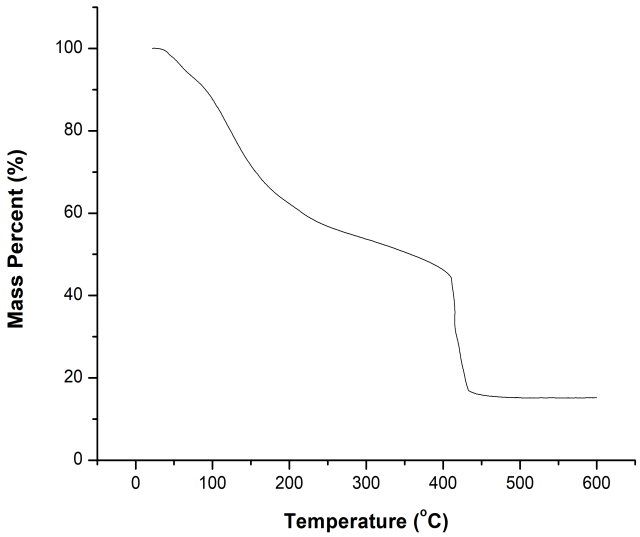


**Fig. S3**: Thermogravimetric analysis of MOF-545.

## 2.4: Nitrogen Adsorption-Desorption Isotherms

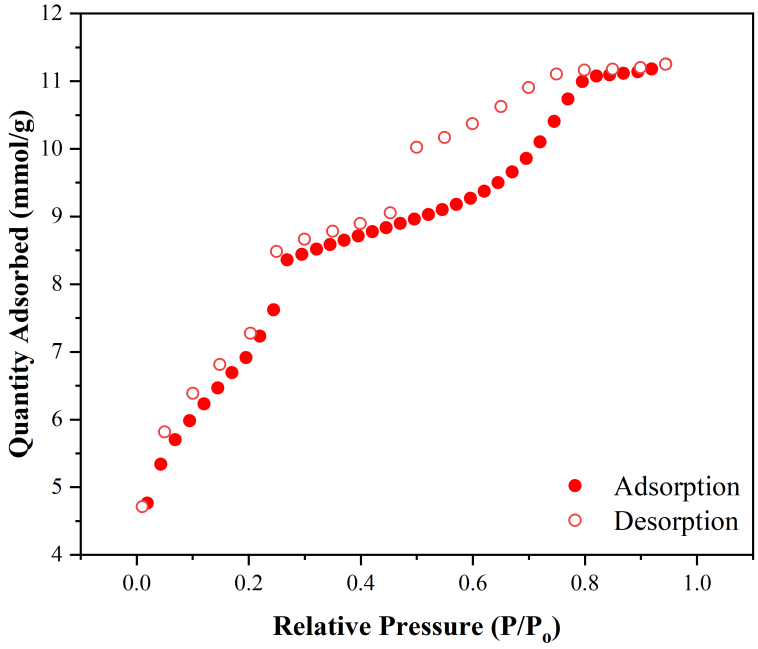


**Fig. S4**: $N_2$ adsorption-desorption isotherms of MOF-545 showing that MOF-545 is a porous material with BET surface area of 759 $m^2\ g^{-1}$, respectively.

## 2.5: UV/Vis Diffuse Reflectance

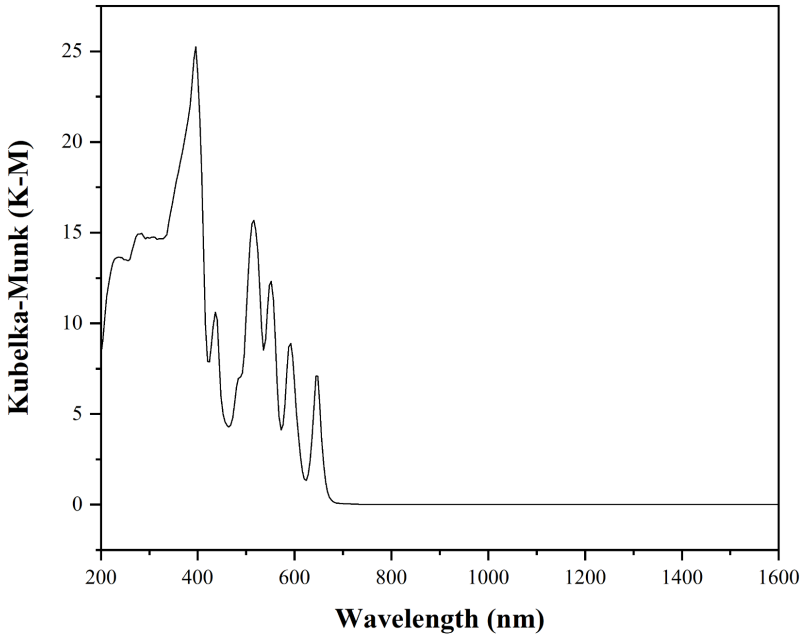


**Fig S5**: UV-Vis diffuse reflectance of MOF-545.

## 3. Computational Details

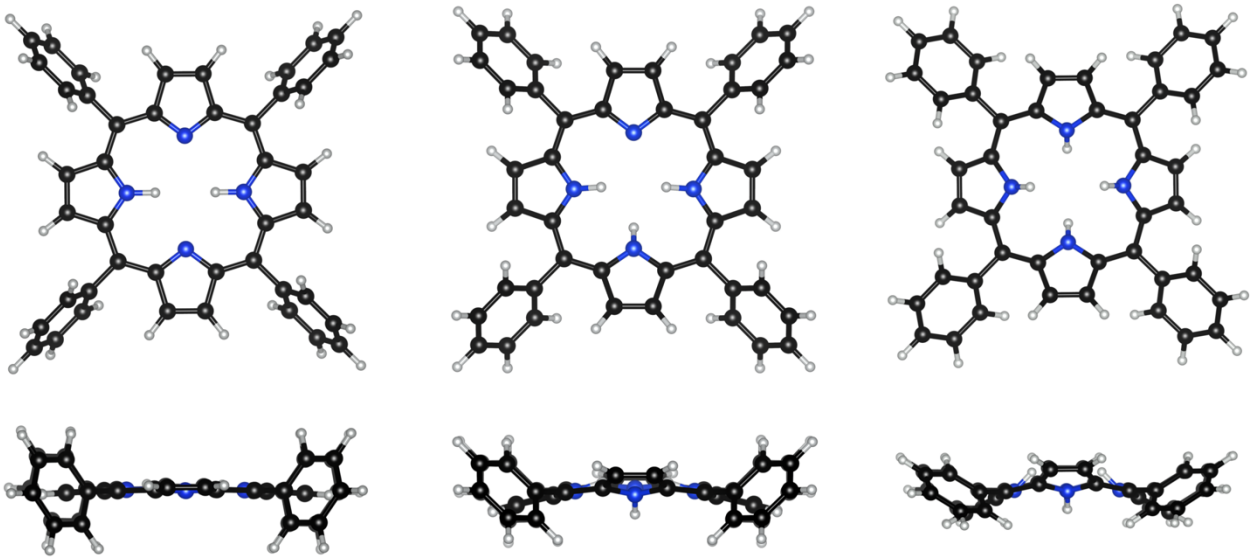

**Fig. S6**: Ground state optimized geometries of neutral tetraphenyl porphyrin, its cation and its dication as calculated using TeraChem[7-9].

Calculated spectra were generated using the cumulant method[2,3], in which $S_0$-$S_1$, $S_0$-$S_2$ and $S_0$-$S_3$ energy gap fluctuations are sampled from ab-intito molecular dynamics trajectories of tetraphenyl porphyrin (TPP), its cation and its dication in vacuum (see Fig. S7). In the cumulant method[2,3], the linear response function due to a single excitation is given by

$$\chi(t) = |\mu|^2 e^{-i\omega_{av}t} exp[-g(t)]$$

where $\boldsymbol{\mu}$ is the transition dipole moment, g(t) the second order cumulant lineshape function that depends on the classical autocorrelation function of excitation energy gap fluctuations and $\omega_{av}$ is the thermal average of the excitation energy. In the standard formulation of the cumulant approach, the Condon approximation is assumed, such that the transition dipole moment is treated as a constant with respect to nuclear degrees of freedom. However, the absorption lineshape of porphyrin in the visible region is known to exhibit strong Herzberg-Teller effects due to an explicit coupling of nuclear degrees of freedom to the transition dipole moment[4]. To include Herzberg-Teller effects in our calculations, we also computed correlation functions of the transition dipole moment fluctuations around its equilibrium value along the MD trajectory. The linear response function is then calculated as:

$$\chi(t) = \left(|\mu_{av}|^2 + C_{\delta\mu}(t)\right) e^{-i\omega_{av}t} exp[-g(t)]$$

Here, $\boldsymbol{\mu}_{av}$ is the average transition dipole moment along the trajectory and $C_{\delta\mu}(t)$ is the quantum autocorrelation function of transition dipole fluctuations around its mean. In accordance with the standard cumulant approach, the quantum autocorrelation function of the dipole fluctuations is constructed from its classical counterpart sampled along the MD trajectory using the harmonic quantum correction factor[6,7]. In this work, we compute response functions for each transition ($S_0$-$S_1$, $S_0$-$S_2$ etc.) individually. The total absorption lineshape is taken as the sum of the contributions from the individual transitions.

Herzberg-Teller effects on absorption spectra of the porphyrins were found to be significant in most cases. For the $S_1$ and $S_2$ states of the dication (H4TPP), the inclusion or exclusion of Herzberg-Teller effects changed the spectra only minorly, but spuriously added long tails to the spectra as noise stemming from the degeneracy of these states. For this reason, Herzberg-Teller effects were not included in this part of the spectrum. Our calculations systematically overestimate the position of the Soret bands relative to the Q-bands. For this reason, calculated Soret bands for all porphyrin species were redshifted by 0.37 eV when comparing to the experimental spectra and predicting the colour.

Molecular dynamics, geometry optimizations, density-functional theory (DFT) and time-dependent density functional theory (TDDFT) calculations were performed with the TeraChem[7-9] quantum chemistry package using the CAM-B3LYP functional[10] and 6-31+G* basis in vacuum at 300 K. For the neutral TPP a total of 22 ps of trajectory data was generated. For the cation and dication, trajectories had a total length of 12 ps. For all trajectories, a Langevin thermostat with collision frequency of 1.0 $ps^{-1}$ was used and the first 2 ps of trajectory were discarded to allow for system equilibration. Because the change in the transition dipole moment due to vibrations in the molecule must be isolated from rotational and translational contributions before calculating Herzberg-Teller contributions to the spectrum, the system and dipole moments were rotated to meet the Eckart conditions[11]. Furthermore, the sign of the transition dipole moment is arbitrary and was adjusted so that the dipole moments form a continuous path along the MD trajectory. It was found that the rotations to Eckart conditions were the most consistent when applied relative to the ground state optimized geometries (Fig S7.5). Additionally, it is possible that two excited states which are close in energy may cross along the MD trajectory, making unambiguous assignments challenging. This is the case in porphyrins, the excitations form pairs of close lying states, e.g. $S_1$ and $S_2$, $S_3$ and $S_4$, etc., and for the dication $S_1$ and $S_2$ become degenerate. These crossings result in discontinuities in the path of the transition dipole moment, and the reform noise in the final generated spectra. It is possible to greatly reduce or remove this noise by sorting the states by dipole moment to give each state the greatest continuity, but this can be difficult. For the cation and dication of porphyrin it was necessary to sample the molecular dynamics trajectory every 1 fs rather than every 2 fs to give the definition required to accurately separate the S1 and S2 states. With this data, spectra were generated using the MolSpecPy package[12].

## 4. Preparation of Acid and Pesticide Samples for UV/vis Measurements

### 4.1. Acid Samples

**Table S1**: Concentration of acid samples

| Concentration (M) | Acid Volume (mL) | MOF Volume (mL) | $H_2O$ Volume (mL) | Total Volume (mL) | MOF Conc. (ppm)* |
|---|---|---|---|---|---|
| 0.01 | 0.03 | 0.1 | 2.87 | 3 | 53.3 |
| 0.05 | 0.15 | 0.1 | 2.75 | 3 | 53.3 |
| 0.1 | 0.3 | 0.1 | 2.6 | 3 | 53.3 |
| 0.2 | 0.6 | 0.1 | 2.3 | 3 | 53.3 |
| 0.3 | 0.9 | 0.1 | 2 | 3 | 53.3 |
| 0.4 | 1.2 | 0.1 | 1.7 | 3 | 53.3 |
| 0.5 | 1.5 | 0.1 | 1.4 | 3 | 53.3 |
| 0.6 | 1.8 | 0.1 | 1.1 | 3 | 53.3 |

*Original concentration of MOF-545 was 1600 PPM.

### 4.2. Glufosinate and Glyphosate Separation

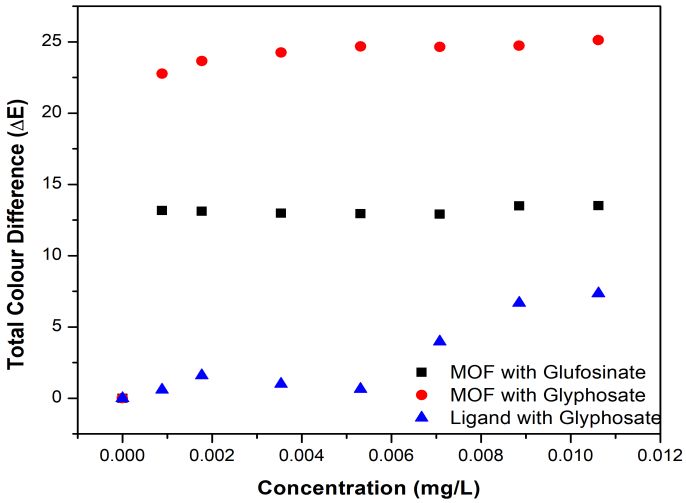


**Fig. S7**: Glufosinate and Glyphosate separation based on their total colour difference (MOF Concentration was 480 ppm, Ligand concentration was 480 ppm).

**Table S2**: Concentrations of glufosinate and glyphosate used in Figure S6.

| **Concentration (mg/L)** | **Glyphosate (ΔE)** | **Glufosinate (ΔE)** | **Ligand with Glyphosate (ΔE)** |
|---|---|---|---|
| $8.85 \times 10^{-4}$ | 22.77 | 13.17 | 0.59 |
| 0.00177 | 23.65 | 13.12 | 1.59 |
| 0.00354 | 24.25 | 12.99 | 1.00 |
| 0.00531 | 24.67 | 12.94 | 0.65 |
| 0.00708 | 24.65 | 1292 | 3.97 |
| 0.00885 | 24.72 | 13.50 | 6.68 |
| 0.0106 | 25.12 | 13.51 | 7.35 |

## 5. MOF-545 Stability

### 5.1. Powder X-ray Diffraction (PXRD)

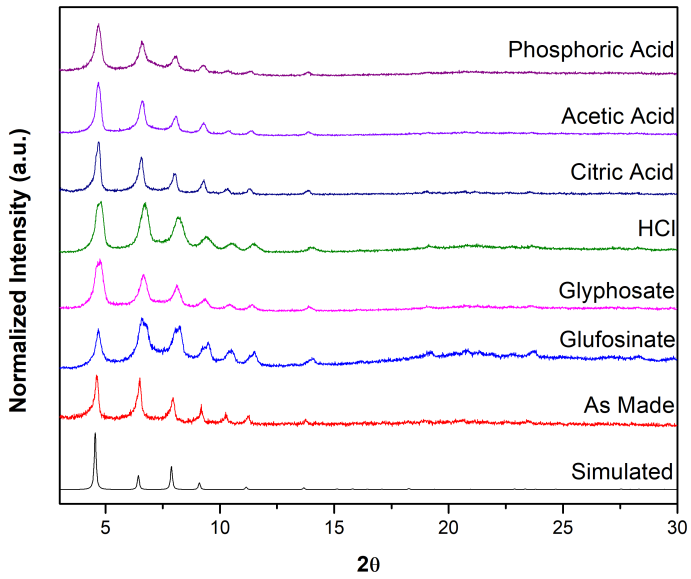


**Fig. S8**: Powder X-ray diffraction patterns of MOF-545 (calculated, black; as made, red) and when it is immersed in solutions with glufosinate (blue), glyphosate (pink), hydrochloric acid (green), Citric Acid (dark blue), Acetic Acid (purple), and Phosphoric Acid (dark purple).

### 5.2. Nitrogen Adsorption-Desorption Isotherms

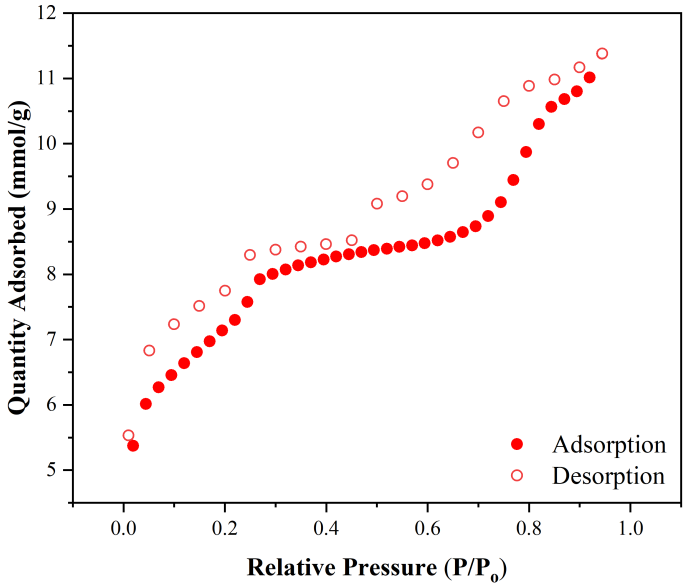


**Fig. S9**: $N_2$ adsorption-desorption isotherms and BET surface areas of MOF-545 after 5 min immersion in Glyphosate solution.

### 5.3. Thermogravimetric Analysis

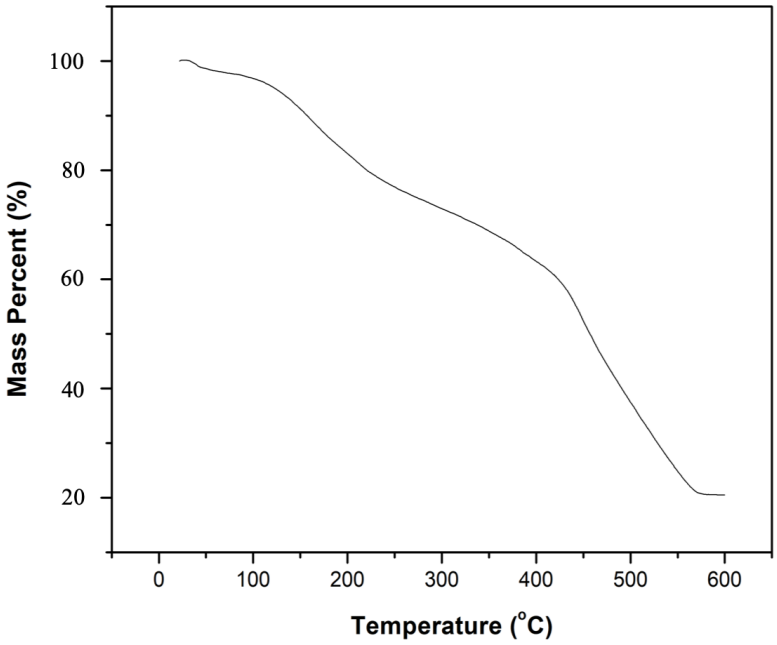


**Fig. S10**: TGA of glyphosate loaded MOF sample.

### 5.4. Fourier-transform Infrared Spectroscopy (FT-IR)

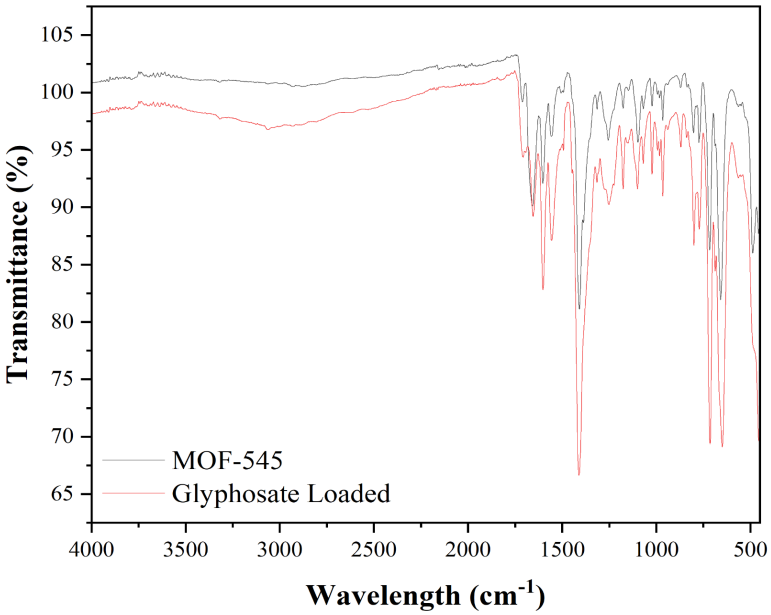


**Fig. S11**: FT-IR of the MOF as synthesized compared to Glyphosate loaded MOF-545.

## 6. Calibration of Glyphosate and Detection Limits

### 6.1. Glyphosate Dilution Series

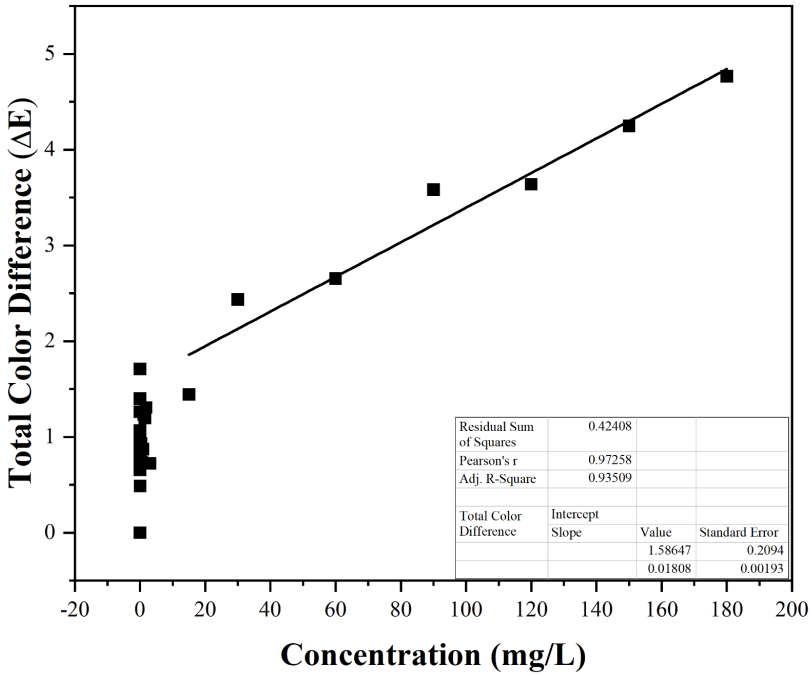


**Fig. S12**: Glyphosate dilution series.

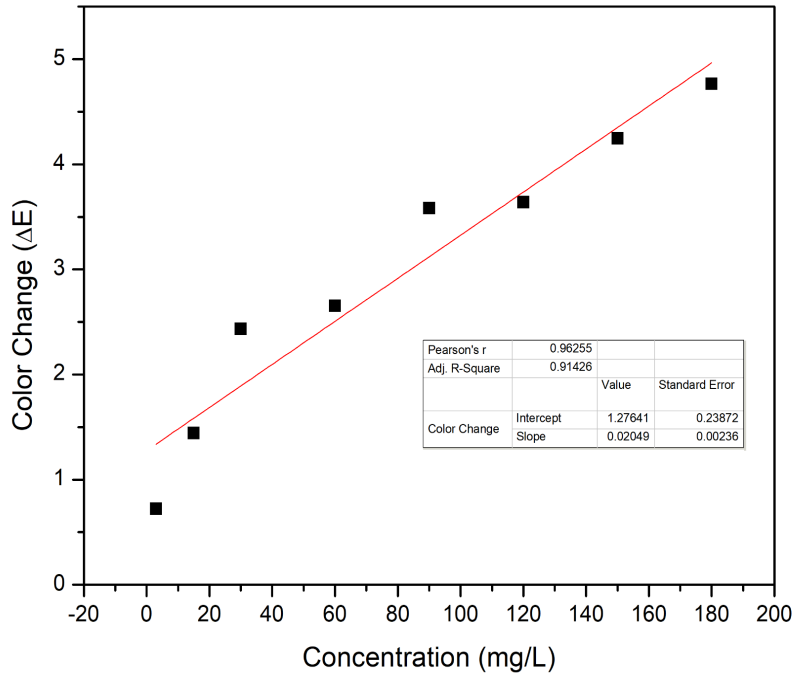


**Fig. S13**: Linear portion of glyphosate dilution series.

**Table S3**: Concentrations and total colour difference (ΔE) for the glyphosate dilution series.

| **Concentration (mg/L)** | **ΔE** | **Concentration (mg/L)** | **ΔE** | **Concentration (mg/L)** | **ΔE** |
|---|---|---|---|---|---|
| 0 | 0.00 | 0.009 | 0.75 | 1.8 | 1.31 |
| 0.00003 | 0.67 | 0.012 | 0.98 | 3 | 0.72 |
| 0.00015 | 1.07 | 0.015 | 1.04 | 15 | 1.44 |
| 0.0003 | 0.66 | 0.018 | 1.71 | 30 | 2.44 |
| 0.0006 | 0.97 | 0.03 | 0.49 | 60 | 2.65 |
| 0.0009 | 0.81 | 0.15 | 0.74 | 90 | 3.58 |
| 0.0012 | 0.72 | 0.3 | 0.93 | 120 | 3.64 |
| 0.0015 | 0.91 | 0.6 | 0.73 | 150 | 4.25 |
| 0.0018 | 1.40 | 0.9 | 0.87 | 180 | 4.77 |
| 0.003 | 0.67 | 1.2 | 1.23 | - | - |
| 0.006 | 0.66 | 1.5 | 1.20 | - | - |

## 7. Water Data

**Table S4**: Concentrations and colour difference (ΔE) for the glyphosate water samples.

| Concentration (mg/L) | Aquafina (ΔE) | Dasani (ΔE) | DI Water (ΔE) | River Water (ΔE) | Tap Water (ΔE) |
|---|---|---|---|---|---|
| 5 | 12.6086 | 10.8320 | 13.5154 | 13.0843 | 11.6522 |
| 10 | 14.0940 | 13.5335 | 13.6844 | 13.1362 | 13.0222 |
| 20 | 14.4705 | 13.8234 | 14.1410 | 13.2570 | 13.4690 |

**Table S5**: Reported concentrations of ions in water sources.

| Water Source | Reported Ions |
|---|---|
| Aquafina[13] | 0.26 mg/L Nitrogen from Nitrate, 0.96 mg/L Sulfate, and 0.0051 mg/L of Trihalomethanes (THMs) |
| Dasani[14] | 0.84 pCi/L Radium 228, 4.2 mg/L chloride, and 0.62 nitrogen from nitrate. According to the Corvallis 2021 |
| Corvallis, OR Tap Water[15] | 0.81 mg/L fluoride, 2 mg/L TOC, 4.0 mg/L chloride, 8.0 mg/L sulfate, 48.7 mg/L alkalinity, 11.8 mg/L Caclium, 11.3 mg/L sodium, 33.8 µg/L THMs, 31.8 µg/L Haloacetic acids, 1.3 mg/L copper, 15 µg/L lead. |
| Willamette River[16] | 0.81 mg/L fluoride, 2 mg/L TOC, 4.0 mg/L chloride, 8.0 mg/L sulfate, 48.7 mg/L alkalinity, 11.8 mg/L Caclium, 11.3 mg/L sodium, 33.8 µg/L THMs, 31.8 µg/L Haloacetic acids, 1.3 mg/L copper, 15 µg/L lead. |

## 8. Comparisons to the Literature

Table S6. Performance of MOF-545 with other benchmark materials[17]

| **Material** | **Colorimetric Method Basis** | **Pesticide** | **Limit of Detection** |
|---|---|---|---|
| Thicholine and $H_2O_2$ sensitive indicators | Enzyme | Chlorpyrifos (Pestanal) | $4.6 \times 10^{-8}$ g $L^{-1}$ |
| MOF-545 | Chemical | Glyphosate | $5.3 \times 10^{-5}$ g $L^{-1}$ |
| Phosphorescent assay based on AuNP | Aptamer | Isocarbophos | $5.40 \times 10^{-7}$ g $L^{-1}$ |
| µPADs | Chemical | Paraoxon ethyl | $2.5 \times 10^{5}$ g $L^{-1}$ |
| Imidazole/AuNPs | Chemical | Diazinon | $3.66 \times 10^{-5}$ g $L^{-1-}$ |
| AuNPs-SF | Enzyme | Chlorpyrifos | $1.0 \times 10^{-5}$ g $L^{-1}$ |
| AchE/choline oxidase enzyme/NPs@ZIF-8 | Chemical | Triazophos | $1.57 \times 10^{-6}$ g $L^{-1}$ |

**9. References**


1. Morris, W.; Volosskiy, B.; Demir, S.; Gándara, F.; McGrier, P. L.; Furukawa, H.; Cascio, D.; Stoddart, J. F.; Yaghi, O. M. Synthesis, Structure, and Metalation of Two New Highly POROUS Zirconium Metal–Organic Frameworks. *Inorg. Chem.* 2012, ***51*** **(12)**, 6443–6445.
2. Mukamel, S.; *Principles of Nonlinear Optical Spectroscopy* (Oxford University Press, New York, 1995).
3. Zuehlsdorff, T. J; Montoya-Castillo, A.; Napoli, J. A.; Markland, T. E.; Isborn, C. M., Optical Spectra in the condensed phase: Capturing anharmonic and vibronic features using dynamic and static approaches. *J. Chem. Phys.* 2019, **151 (7)**, 074111.
4. Santoro, F.; Lami, A.; Improta, R.; Bloino, J.; Barone, V., Effective method for the computation of optical spectra of large molecules at finite temperature including the Duschinsky and Herzberg-Teller effect: The $Q_x$ band of porphyin as a case study. *J. Chem. Phys.* 2008, **128 (22)**, 224311.
5. Craig, I. R.; Manolopoulos, D. E., Ouantum statistics and classical mechanics: Real time correlation functions from ring polymer molecular dynamics. *J. Chem. Phys.* 2004, **121**, 3368.
6. Ramirez, R.; Lopez-Ciudad, T.; Padma Kumar, P.; Marx, D., Quantum corrections to classical time-correlation functions: Hydrogen bonding and anharmonic floppy modes, *J. Chem. Phys.* 2004, **121**, 3973.
7. Ufimtsev, I. S.; Martinez, T. J., Quantum chemistry on graphical processing units. 3. Analytical energy gradients and first principles molecular dynamics. *J. Chem. Theory Comput.* 2009, **5**, 3619-2628.
8. Titov, A. V.; Ufimtsev, I. S.; Luehr, N.; Martinez, T. J., Generating efficient quantum chemistry codes for novel architectures. *J. Chem. Theory Comput.* 2013, **9**, 213-221.
9. Isborn, C. M.; Luehr, N.; Ufimtsev, I. S.; Martinez, T. J., Excited state electronic structure with configuration interaction singles and Tamm-Dancoff time-dependent dnesity functional theory on graphical processing units. *J. Chem. Theory Comput.* 2011, 7, 1814-1823.
10. Yanai, T.; Tew, D. P.; Handy, N. C., A new hybrid exchange-correlation functional using the Coulomb-attenuating method (CAM-B3LYP). *Chem. Phys. Lett.* 2004, **393**, 51-57 (2004).
11. Szalay, V., Eckart-Sayvetz conditions revisited. *J. Chem. Phys.* 2014, **140 (23)**, 234107.
12. T. J. Zuehlsdorff, "MolSpeckPy: Spectroscopy Python Code", available on GitHub: https://github.com/tjz21/spectroscopy_python_code (2021)
13. Aquafina Bottled Water Information, https://www.aquafina.com/pdf/bottledWaterInformation_en.pdf, (accessed July 2021)
14. Dasani Annual Analysis, https://www.dasani.com/content/dam/nagbrands/us/dasani/en/home/water-analysis-report-2019.pdf, (accessed July 2021)
15. 2021 Water Quality Report, https://archives.corvallisoregon.gov/public/ElectronicFile.aspx?dbid=0&docid=2213993, (accessed July 2021).
16. More Information About The Willamette River Report Card Toxics Indicator, https://www.oregon.gov/deq/FilterDocs/WillToxicsRpt.pdf, (accessed July 2021)
17. Bhattu, M.; Verma, M.; Kathuria, D. Recent Advancements in the Detection of Organophosphate Pesticides: A Review. *Anal. Methods* 2021, ***13*** **(38),** 4390–4428.